

# Strong interlayer coupling in van der Waals heterostructures built from single-layer chalcogenides

Hui Fang<sup>a,b</sup>, Corsin Battaglia<sup>a,b</sup>, Carlo Carraro<sup>c</sup>, Slavomir Nemsak<sup>b,d</sup>, Burak Ozdol<sup>e,f</sup>, Jeong Seuk Kang<sup>a,b</sup>, Hans A. Bechtel<sup>g</sup>, Sujay B. Desai<sup>a,b</sup>, Florian Kronast<sup>h</sup>, Ahmet A. Unal<sup>h</sup>, Giuseppina Conti<sup>b,d</sup>, Catherine Conlon<sup>b,d</sup>, Gunnar K. Palsson<sup>b,d</sup>, Michael C. Martin<sup>g</sup>, Andrew M. Minor<sup>e,f</sup>, Charles S. Fadley<sup>b,d</sup>, Eli Yablonovitch<sup>a,b,1</sup>, Roya Maboudian<sup>c</sup>, and Ali Javey<sup>a,b,1</sup>

Departments of <sup>a</sup>Electrical Engineering and Computer Sciences, <sup>c</sup>Chemical and Biomolecular Engineering, and <sup>e</sup>Materials Science and Engineering, University of California, Berkeley, CA 94720; <sup>b</sup>Materials Sciences Division, <sup>f</sup>National Center for Electron Microscopy, and <sup>g</sup>Advanced Light Source, Lawrence Berkeley National Laboratory, Berkeley, CA 94720; <sup>d</sup>Department of Physics, University of California, Davis, CA 95616; and <sup>h</sup>Helmholtz-Zentrum Berlin für Materialien und Energie GmbH, D-12489 Berlin, Germany

Contributed by Eli Yablonovitch, March 24, 2014 (sent for review March 10, 2014)

Semiconductor heterostructures are the fundamental platform for many important device applications such as lasers, light-emitting diodes, solar cells, and high-electron-mobility transistors. Analogous to traditional heterostructures, layered transition metal dichalcogenide heterostructures can be designed and built by assembling individual single layers into functional multilayer structures, but in principle with atomically sharp interfaces, no interdiffusion of atoms, digitally controlled layered components, and no lattice parameter constraints. Nonetheless, the optoelectronic behavior of this new type of van der Waals (vdW) semiconductor heterostructure is unknown at the single-layer limit. Specifically, it is experimentally unknown whether the optical transitions will be spatially direct or indirect in such hetero-bilayers. Here, we investigate artificial semiconductor heterostructures built from single-layer WSe<sub>2</sub> and MoS<sub>2</sub>. We observe a large Stokes-like shift of ~100 meV between the photoluminescence peak and the lowest absorption peak that is consistent with a type II band alignment having spatially direct absorption but spatially indirect emission. Notably, the photoluminescence intensity of this spatially indirect transition is strong, suggesting strong interlayer coupling of charge carriers. This coupling at the hetero-interface can be readily tuned by inserting dielectric layers into the vdW gap, consisting of hexagonal BN. Consequently, the generic nature of this interlayer coupling provides a new degree of freedom in band engineering and is expected to yield a new family of semiconductor heterostructures having tunable optoelectronic properties with customized composite layers.

MoS<sub>2</sub>-WSe<sub>2</sub> heterostructure | Moiré pattern | charge transfer | exciton relaxation | rectifying

Two-dimensional layered transition metal dichalcogenide (TMDC) semiconductors such as MoS<sub>2</sub> and WSe<sub>2</sub> have established themselves as strong contenders for next-generation electronics and optoelectronics (1–6) and are promising building blocks for novel semiconductor heterostructures (7–11). Conventional heterostructures are mainly based on group IV, III–V, or II–VI semiconductors with covalent bonding between atoms at the hetero-interface. Owing to atomic interdiffusion during growth, the resulting atomic-scale interface roughness and composition variation at the hetero-interface inevitably smear the density of states profile and consequently compromise the performance of these heterostructures, especially as the film thicknesses are reduced toward a single atomic layer. In addition, the choice of material components for conventional heterostructures is strongly dictated by lattice mismatch.

In TMDCs, however, individual layers are held together by van der Waals (vdW) forces, without surface dangling bonds (12). Semiconductor heterostructures built up from monolayer TMDCs would in principle offer atomically regulated interfaces and thereby sharp band edges. Theoretical studies have predicted different

electronic structures and optical properties from TMDC hetero-bilayers (13–17); however, to date there have been no experimental results. Whereas previous experimental efforts have focused on graphene-based layered heterostructures (8–11, 18–26), we present an experimental study on the electronic interlayer interaction in a heterostructure built from two single-layer TMDC semiconductors, namely, MoS<sub>2</sub> and WSe<sub>2</sub>. The hetero-bilayers are characterized by transmission electron microscopy, X-ray photoelectron microscopy, electron transport studies, and optical spectroscopy to elucidate the band alignments, optoelectronic properties, and the degree of the electronic layer coupling in this novel material system.

The fabrication of WSe<sub>2</sub>/MoS<sub>2</sub> hetero-bilayers was realized by stacking individual monolayers on top of each other (see *SI Methods* for details). Fig. 1*A* shows an illustration of the hetero-bilayer, and Fig. 1*B* displays the corresponding optical microscope image of a WSe<sub>2</sub>/MoS<sub>2</sub> hetero-bilayer on a Si substrate with 260-nm thermally grown SiO<sub>2</sub>. Owing to the 3.8% lattice mismatch, estimated from the bulk lattice constants (12), as well as the unregulated, but in principle controllable, angular alignment ( $\phi$ ) between the constituent layers, the heterostructure lattice forms a moiré pattern, clearly visible in the high-resolution transmission electron microscopy (HRTEM) image in Fig. 1*C*. The HRTEM image displays the boundary region between

## Significance

A new class of heterostructures consisting of layered transition metal dichalcogenide components can be designed and built by van der Waals (vdW) stacking of individual monolayers into functional multilayer structures. Nonetheless, the optoelectronic properties of this new type of vdW heterostructure are unknown. Here, we investigate artificial semiconductor heterostructures built from single-layer WSe<sub>2</sub> and MoS<sub>2</sub>. We observe spatially direct absorption but spatially indirect emission in this heterostructure, with strong interlayer coupling of charge carriers. The coupling at the hetero-interface can be readily tuned by inserting hexagonal BN dielectric layers into the vdW gap. The generic nature of this interlayer coupling is expected to yield a new family of semiconductor heterostructures having tunable optoelectronic properties through customized composite layers.

Author contributions: H.F., C. Carraro, R.M., and A.J. designed research; H.F., C. Carraro, S.N., B.O., J.S.K., H.A.B., S.B.D., F.K., A.A.U., G.C., C. Conlon, G.K.P., and M.C.M. performed research; H.F., C.B., C. Carraro, S.N., B.O., G.C., A.M.M., C.S.F., E.Y., R.M., and A.J. analyzed data; and H.F., C.B., and A.J. wrote the paper.

The authors declare no conflict of interest.

Freely available online through the PNAS open access option.

<sup>1</sup>To whom correspondence may be addressed. E-mail: eliy@eecs.berkeley.edu or ajavey@eecs.berkeley.edu.

This article contains supporting information online at [www.pnas.org/lookup/suppl/doi:10.1073/pnas.1405435111/-DCSupplemental](http://www.pnas.org/lookup/suppl/doi:10.1073/pnas.1405435111/-DCSupplemental).

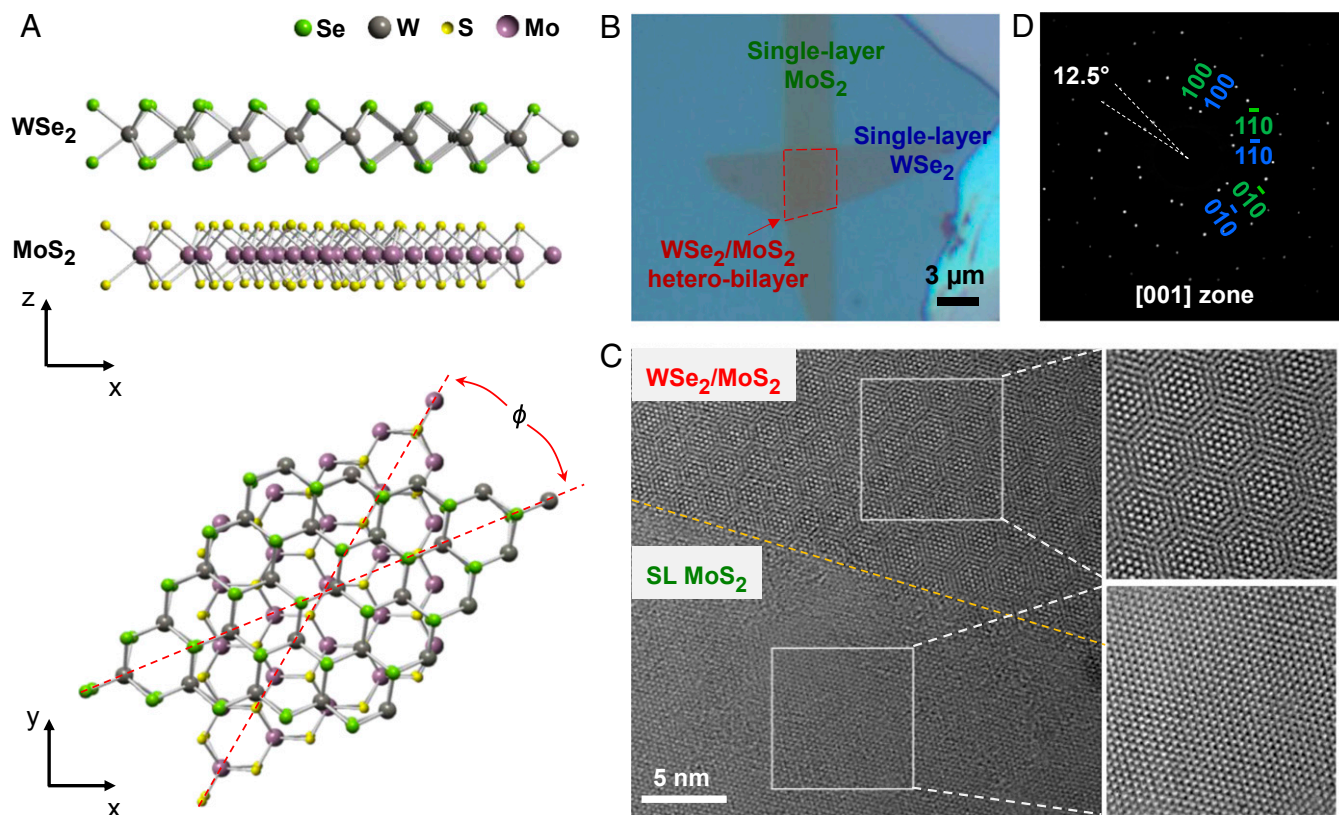


**Fig. 1.**  $\text{WSe}_2/\text{MoS}_2$  hetero-bilayer illustration, optical image, and TEM images. (A) Atomistic illustrations of the heterostructure of single-layer (SL)  $\text{WSe}_2$  on SL  $\text{MoS}_2$  with their respective lattice constants and a misalignment angle  $\phi$ . (B) Optical microscope image of a  $\text{WSe}_2/\text{MoS}_2$  hetero-bilayer on a  $\text{Si}/\text{SiO}_2$  substrate (260-nm  $\text{SiO}_2$ ). (C) HRTEM images of a boundary region of SL  $\text{MoS}_2$  and the hetero-bilayer, showing the resulting Moiré pattern. (D) The electron diffraction pattern of the hetero-bilayer shown in B, with the pattern of  $\text{MoS}_2$  and  $\text{WSe}_2$  indexed in green and blue colors, respectively.

single-layer  $\text{MoS}_2$  and the  $\text{WSe}_2/\text{MoS}_2$  hetero-bilayer. Whereas  $\text{MoS}_2$  exhibits a simple hexagonal lattice, the heterostructure shows moiré fringes with a spatial envelope periodicity on the order of four to six times the lattice constants of  $\text{WSe}_2$  (or  $\text{MoS}_2$ ). Inspection of the diffraction pattern in Fig. 1D along the [001] zone axis reveals that in this particular sample the two hexagonal reciprocal lattices are rotated by  $\phi=12.5^\circ$  with respect to each other and there is negligible strain in the two constituent layers (*Supporting Information*). The alignment of the two lattices can also be examined with a fast Fourier transform of the two zoomed-in TEM images in Fig. 1C (Fig. S1). The absence of strain in the constituent layers of the  $\text{WSe}_2/\text{MoS}_2$  hetero-bilayer is also confirmed by Raman spectroscopy (Fig. S2), which show that the in-plane vibration modes of both  $\text{WSe}_2$  and  $\text{MoS}_2$  maintain their corresponding positions before and after transfer.

To shed light on the electronic structure of the  $\text{WSe}_2/\text{MoS}_2$  heterostack, we performed X-ray photoelectron spectroscopy (XPS). Specifically, we used a photoemission electron microscope (PEEM) with a high spatial resolution of 30 nm to discriminate between photoelectrons emitted from the  $\text{WSe}_2$  single layer,  $\text{MoS}_2$  single layer, and the  $\text{WSe}_2/\text{MoS}_2$  hetero-bilayer, as illustrated in Fig. 2A (see Fig. S3 for details). In addition, by looking at the core-level photoelectrons, we achieved elemental and electronic selectivity that allows us to probe photoelectrons originating from the top layer of the hetero-bilayer and to directly quantify the potential difference between the  $\text{WSe}_2$  layer in the hetero-stack with respect to the  $\text{WSe}_2$  single-layer reference on the substrate. As shown in Fig. 2B, a peak shift of about  $-220$  meV in binding energy (or  $+220$  meV in kinetic energy) is evident in the W 4f core levels of the hetero-bilayer compared with the  $\text{WSe}_2$  single layer. The direction of the peak shift is

consistent with a negative net charge on the  $\text{WSe}_2$  in the  $\text{WSe}_2/\text{MoS}_2$  hetero-bilayer. However, a shift of  $+190$  meV is observed in the Mo 3d core levels of the  $\text{WSe}_2/\text{MoS}_2$  in Fig. 2C. Our PEEM results therefore indicate that the  $\text{WSe}_2$  layer has a negative net charge, whereas the  $\text{MoS}_2$  layer has a positive net charge as a result of contact potential. The hetero-bilayer can essentially be interpreted as being a 2D dipole, an atomically thin parallel plate capacitor with vdW gap with a built-in potential up to 400 meV, originating from the work function difference induced charge transfer between the two constituent single layers. The latter interpretation is also consistent with the p- and n-type character of  $\text{WSe}_2$  and  $\text{MoS}_2$ , respectively (2, 3).

To investigate the optoelectronic properties of the  $\text{WSe}_2/\text{MoS}_2$  hetero-bilayer, we used photoluminescence (PL) and absorption spectroscopy. It is known that both single-layer  $\text{WSe}_2$  and  $\text{MoS}_2$  exhibit direct band gaps, whereas their bulk and homo-bilayer counterparts are indirect (1, 27). In agreement with previous work we observe strong excitonic PL peaks at 1.64 eV and 1.87 eV for single-layer  $\text{WSe}_2$  and  $\text{MoS}_2$ , respectively (Fig. 3A). Note that single-layer  $\text{WSe}_2$  shows a 10–20 times higher PL intensity than single-layer  $\text{MoS}_2$ , a result consistent with ref. 28. For the  $\text{WSe}_2/\text{MoS}_2$  hetero-bilayer, we observe a peak at 1.55 eV, lying interestingly at a lower energy than for the two constituent single layers, as shown in Fig. 3A (with intensity  $\sim 1.5$  times higher than for single-layer  $\text{MoS}_2$ ). The appearance of a peak at such low energy was observed consistently for multiple ( $>10$ ) samples, with peak energies ranging from 1.50 to 1.56 eV (Fig. S4). This distribution is attributed to sample-to-sample variations in interface quality and/or alignment angle  $\phi$ . Of value in optoelectronics, an Urbach tail inverse slope, corresponding to the band edge sharpness of  $\sim 30$  meV/dec is extracted

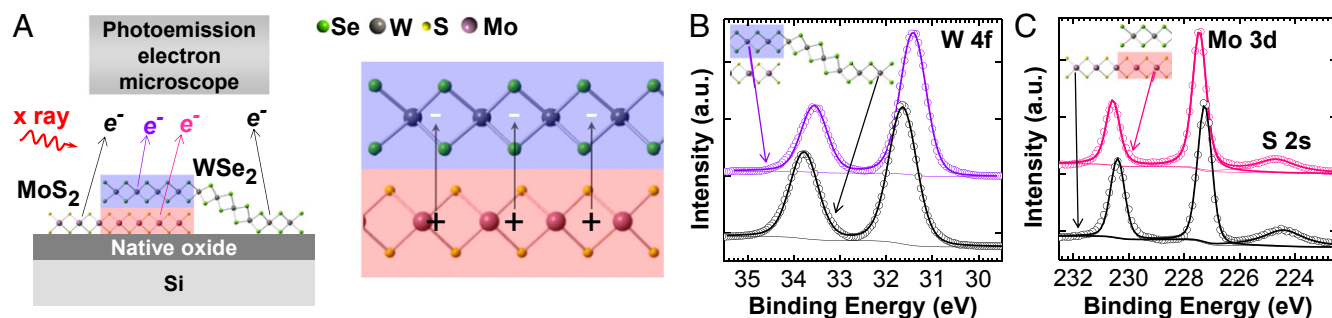


**Fig. 2.** XPS core level shift analyses of  $\text{WSe}_2/\text{MoS}_2$  heterostructures. (A) Sketch of the spatially resolved PEEM experiment. (B) Comparison of W 4f core level doublet from  $\text{WSe}_2$  and  $\text{WSe}_2/\text{MoS}_2$  indicating a 220-meV shift to lower binding energy, corresponding to a negative net charge on the  $\text{WSe}_2$  top layer. (C) Comparison of Mo 3d core level doublet and S 2s singlet from  $\text{MoS}_2$  and  $\text{WSe}_2/\text{MoS}_2$  indicating a shift of 190 meV to higher binding energy, corresponding to a positive net charge on  $\text{MoS}_2$ . The single peak at 224.4–224.6 eV is identified as S 2s, which shows the same shift as Mo 3d, as expected.

from the PL spectra (29, 30) (Fig. S5). The steep tail slopes of our hetero-bilayer prove that high-quality heterostructures with sharp band edges can be built at the single-layer limit using TMDC building blocks, which is a unique feature of this material system.

The nature of the photoluminescence of the  $\text{WSe}_2/\text{MoS}_2$  hetero-bilayer is intriguing. To better understand the electronic structure of the hetero-bilayer, we performed absorption measurements in the near-infrared and visible part of the spectrum using synchrotron light shown as dashed lines in Fig. 3B. The  $\text{WSe}_2/\text{MoS}_2$  hetero-bilayer shows a first absorption peak at 1.65 eV and a second peak at 1.91 eV. These peaks closely coincide with the absorption peaks of single-layer  $\text{WSe}_2$  and  $\text{MoS}_2$ ,

respectively. Interestingly, comparing the absorption spectra with the normalized PL data shown in Fig. 3B, we note that the hetero-bilayer exhibits a striking  $\sim 100$  meV shift between the PL and absorbance peaks. This large Stokes-like shift is consistent with a spatially indirect transition in a staggered gap (type II) heterostructure (31) (as shown in Fig. 3C). Our hetero-bilayers share certain similarities with organic semiconductor heterostructures in which donor and acceptor layers are also bound by weak intermolecular vdW forces (32). Similar to the optical processes in organic heterostructures, photons are absorbed in single-layer  $\text{WSe}_2$  and single-layer  $\text{MoS}_2$ , generating excitons in both layers. Photo-excited excitons then relax at the  $\text{MoS}_2/\text{WSe}_2$

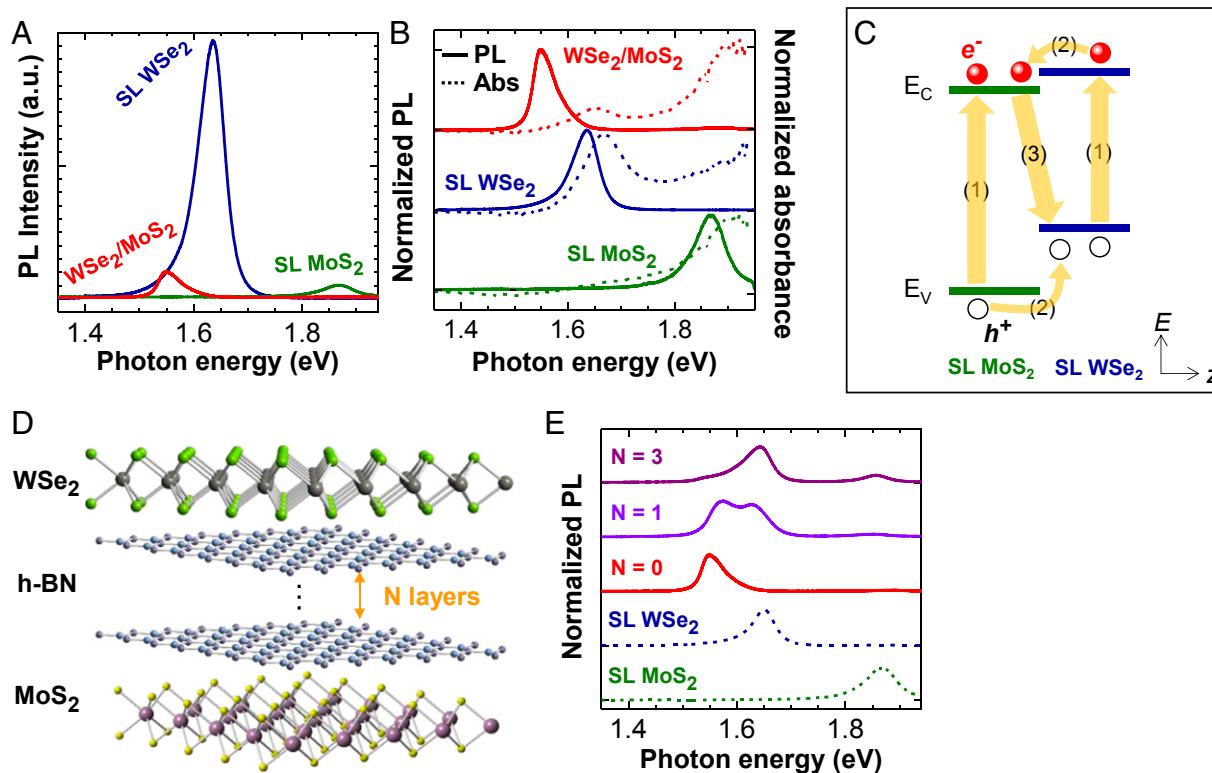


**Fig. 3.** Photoluminescence and absorption from  $\text{WSe}_2/\text{MoS}_2$  hetero-bilayers. (A) PL spectra of single-layer  $\text{WSe}_2$ ,  $\text{MoS}_2$ , and the corresponding hetero-bilayer. (B) Normalized PL (solid lines) and absorbance (dashed lines) spectra of single-layer  $\text{WSe}_2$ ,  $\text{MoS}_2$ , and the corresponding hetero-bilayer, where the spectra are normalized to the height of the strongest PL/absorbance peak. (C) Band diagram of  $\text{WSe}_2/\text{MoS}_2$  hetero-bilayer under photo excitation, depicting (1) absorption and exciton generation in  $\text{WSe}_2$  and  $\text{MoS}_2$  single layers, (2) relaxation of excitons at the  $\text{MoS}_2/\text{WSe}_2$  interface driven by the band offset, and (3) radiative recombination of spatially indirect excitons. (D) An atomistic illustration of the heterostructure of single-layer  $\text{WSe}_2$ /single-layer  $\text{MoS}_2$  with few-layer h-BN spacer in the vdW gap. (E) Normalized PL spectra from single-layer  $\text{WSe}_2$ /single-layer  $\text{MoS}_2$  heterostructure with  $n$  layers of h-BN ( $n = 0, 1$ , and  $3$ ).



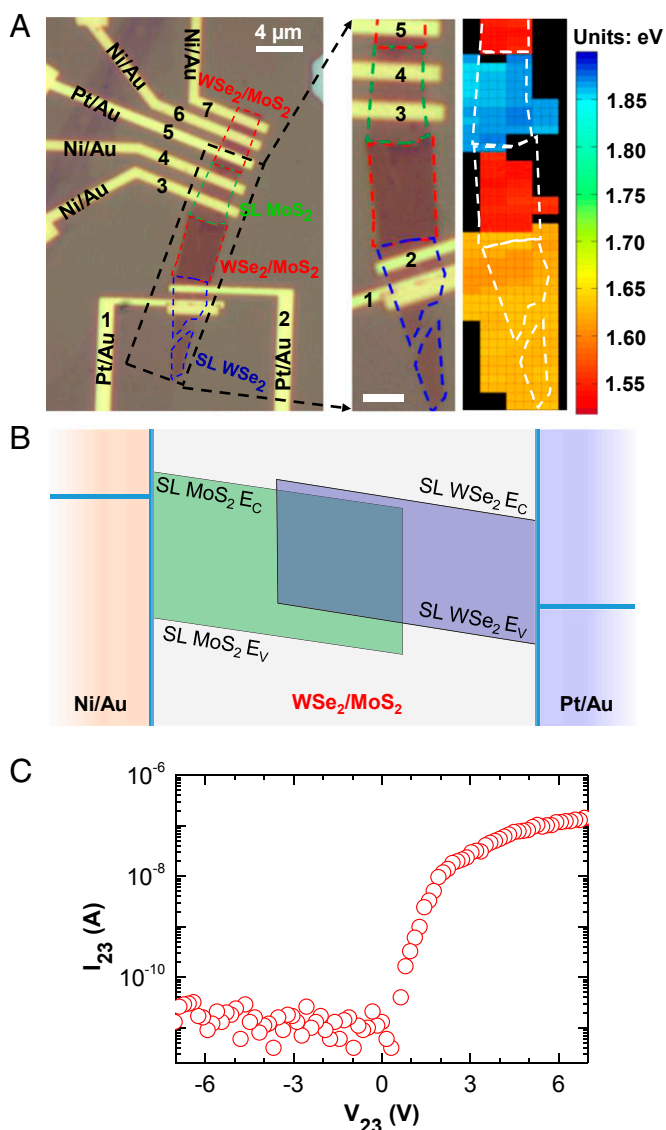


**Fig. 4.** Electrical transport across the  $\text{WSe}_2/\text{MoS}_2$  hetero-interface. (A) Optical micrograph image of a device encompassing single-layer  $\text{WSe}_2$ ,  $\text{WSe}_2/\text{MoS}_2$  hetero-bilayer, and single-layer  $\text{MoS}_2$  on a  $\text{Si}/\text{SiO}_2$  substrate. Electrodes are numbered 1–7 from bottom to top. (Right) A color-coded PL peak energy map. (Scale bar, 2  $\mu\text{m}$ .) (B) A qualitative band diagram of the single-layer  $\text{WSe}_2$ /hetero-bilayer/single-layer  $\text{MoS}_2$  device, corresponding to the device between electrodes 2 and 3. (C) I–V characteristic when measuring between electrodes 2 and 3, with 2 grounded and 3 biased. A back-gate voltage of 50 V was applied to reduce the contact resistance to  $\text{MoS}_2$  and patterned  $\text{NO}_2$  doping was used near the  $\text{WSe}_2$  contact for reducing the contact resistance.

interface, driven by the band offset as shown in Fig. 3C. That band offset is also consistent with the measured built-in electric field from PEEM. Owing to the energy lost to the band offset (Fig. 3C), the PL excitonic peak energy is lower than the excitonic band gaps of either material component. This 100-meV shift may be a balance between conduction band offset between the two monolayers versus diminished exciton binding energy associated with being spatially indirect. Note that in the hetero-bilayer we observe only a weak luminescence signal at the energies corresponding to the excitonic band gaps of single-layer  $\text{MoS}_2$  and  $\text{WSe}_2$ , suggesting that the large majority of the photo-excited carriers are relaxed at the interface producing the highest luminescence for the spatially indirect recombination process.

To fine-tune the interlayer interaction in the  $\text{WSe}_2/\text{MoS}_2$  hetero-bilayer, single- and few-layer sheets of hexagonal BN (h-BN) spacer layers were inserted into the vdW gap (Fig. 3D) using the same transfer technique. Fig. 3E shows the normalized PL of hetero-stacks with single- and trilayer h-BN spacers. Interlayer spatially indirect recombination becomes negligible for the sample with a trilayer h-BN spacer, as indicated by both the position and the intensity of the peak at 1.64 eV (Fig. 3E and Fig. S6), which are nearly the same as for single-layer  $\text{WSe}_2$ . However, a single layer of h-BN does not fully suppress the interlayer interaction between  $\text{WSe}_2$  and  $\text{MoS}_2$ . The results demonstrate that the interlayer coupling can be readily tuned by intercalation of dielectric layers and provide yet another degree of control in the vdW heterostructure properties.

Finally, we explored the carrier transport along the hetero-bilayer interface. A single flake consisting of single-layer  $\text{WSe}_2$  and  $\text{MoS}_2$ , and an overlapping hetero-bilayer was made via the transfer process. The flake was dry etched into a long ribbon (Fig. 4A). A corresponding PL peak energy map is shown at the right edge of Fig. 4A, further depicting the ribbon structure by color coding of the luminescence energy. Multiple source/drain (S/D) metal electrodes were then fabricated by electron beam lithography and lift-off on each region of the ribbon (see Figs. S7 and S8 for details). The  $\text{Si}/\text{SiO}_2$  substrate serves as the global back gate, with 260 nm gate oxide thickness. As expected single-layer  $\text{MoS}_2$  and  $\text{WSe}_2$  devices exhibit n- and p-channel characteristics, respectively (Fig. S9), consistent with previous reports (2, 3). However, the device consisting of one contact on the monolayer  $\text{WSe}_2$  and the other on monolayer  $\text{MoS}_2$ , with the two layers overlapping in the central region (Fig. 4B) exhibits a distinct rectifying behavior (Fig. 4C and Fig. S10), consistent with type II band alignment of the hetero-bilayer. The rectification provides additional evidence for electrical coupling and proper contact potential between the two constituent layers. This behavior is consistent with previous work on TMDC/nanotubes (33) and TMDC/III-V heterostructures (34), which had shown that electrically active vdW interfaces can be achieved from TMDC components. The work here highlights the ability to engineer a novel class of electronic and optoelectronic devices by vdW stacking of the desired layered chalcogenide components with molecular-scale thickness control.

In summary, we have fabricated and characterized an artificial vdW heterostructure by stacking monolayer TMDC building blocks and achieved electronic coupling between the two 2D semiconductor constituents. Strong PL with a large Stokes-like shift was observed from the  $\text{WSe}_2/\text{MoS}_2$  hetero-bilayer, consistent with spatially indirect luminescence from a type II heterostructure. We anticipate that our result will trigger subsequent studies focused on the bottom-up creation of new heterostructures by varying chemical composition, interlayer spacing, and angular alignment. In addition, the focus will be on the fabrication of vdW semiconductor heterostructure devices with tuned optoelectronic properties from customized single-layer components. Particularly, electroluminescence efficiency of vdW heterostructures needs to be explored experimentally to examine their viability for use as nanoscale light-emitting/lasing devices.

**ACKNOWLEDGMENTS.** Materials characterization of this work was supported by the director, Office of Science, Office of Basic Energy Sciences, Materials Sciences and Engineering Division of the US Department of Energy (DOE) under Contract DE-AC02-05CH11231. The device fabrication and characterization was supported by the National Science Foundation (NSF) E<sup>2</sup>S center. The transmission electron microscopy work was performed at the National Center for Electron Microscopy, Lawrence Berkeley National Laboratory, which is supported by US DOE Contract DE-AC02-05CH11231. The absorption measurements were performed at the Advanced Light Source, Lawrence Berkeley National Laboratory. C. Carraro and R.M. acknowledge support from NSF Grant EEC-0832819 (Center of Integrated Nanomechanical Systems).

1. Mak KF, Lee C, Hone J, Shan J, Heinz TF (2010) Atomically thin  $\text{MoS}_2$ : A new direct-gap semiconductor. *Phys Rev Lett* 105(13):136805.
2. Radisavljevic B, Radenovic A, Brivio J, Giacometti V, Kis A (2011) Single-layer  $\text{MoS}_2$  transistors. *Nat Nanotechnol* 6(3):147–150.
3. Fang H, et al. (2012) High-performance single layered  $\text{WSe}_2$  p-FETs with chemically doped contacts. *Nano Lett* 12(7):3788–3792.
4. Wang H, et al. (2012) Integrated circuits based on bilayer  $\text{MoS}_2$  transistors. *Nano Lett* 12(9):4674–4680.
5. Zeng H, Dai J, Yao W, Xiao D, Cui X (2012) Valley polarization in  $\text{MoS}_2$  monolayers by optical pumping. *Nat Nanotechnol* 7(8):490–493.
6. Jones AM, et al. (2013) Optical generation of excitonic valley coherence in monolayer  $\text{WSe}_2$ . *Nat Nanotechnol* 8(9):634–638.
7. Geim AK, Grigorieva IV (2013) Van der Waals heterostructures. *Nature* 499(7459):419–425.
8. Yu WJ, et al. (2013) Vertically stacked multi-heterostructures of layered materials for logic transistors and complementary inverters. *Nat Mater* 12(3):246–252.
9. Georgiou T, et al. (2013) Vertical field-effect transistor based on graphene- $\text{WS}_2$  heterostructures for flexible and transparent electronics. *Nat Nanotechnol* 8(2):100–103.
10. Yu WJ, et al. (2013) Highly efficient gate-tunable photocurrent generation in vertical heterostructures of layered materials. *Nat Nanotechnol* 8(12):952–958.
11. Britnell L, et al. (2013) Strong light-matter interactions in heterostructures of atomically thin films. *Science* 340(6138):1311–1314.
12. Wilson J, Yoffe A (1969) The transition metal dichalcogenides discussion and interpretation of the observed optical, electrical and structural properties. *Adv Phys* 18(73):193–335.
13. Terrones H, López-Urías F, Terrones M (2013) Novel hetero-layered materials with tunable direct band gaps by sandwiching different metal disulfides and diselenides. *Sci Rep* 3:1549.
14. Kang J, Li J, Li S-S, Xia J-B, Wang L-W (2013) Electronic structural Moiré pattern effects on  $\text{MoS}_2/\text{MoSe}_2$  2D heterostructures. *Nano Lett* 13(11):5485–5490.
15. Kośmider K, Fernández-Rossier J (2013) Electronic properties of the  $\text{MoS}_2$ - $\text{WS}_2$  heterojunction. *Phys Rev B* 87(7):075451.
16. Komsa H-P, Krasheninnikov AV (2013) Electronic structures and optical properties of realistic transition metal dichalcogenide heterostructures from first principles. *Phys Rev B* 88(8):085318.
17. Gong C, et al. (2013) Band alignment of two-dimensional transition metal dichalcogenides: Application in tunnel field effect transistors. *Appl Phys Lett* 103(5):053513.
18. Dean CR, et al. (2010) Boron nitride substrates for high-quality graphene electronics. *Nat Nanotechnol* 5(10):722–726.
19. Ponomarenko L, et al. (2011) Tunable metal-insulator transition in double-layer graphene heterostructures. *Nat Phys* 7(12):958–961.
20. Haigh SJ, et al. (2012) Cross-sectional imaging of individual layers and buried interfaces of graphene-based heterostructures and superlattices. *Nat Mater* 11(9):764–767.
21. Britnell L, et al. (2012) Field-effect tunneling transistor based on vertical graphene heterostructures. *Science* 335(6071):947–950.
22. Gorbachev R, et al. (2012) Strong Coulomb drag and broken symmetry in double-layer graphene. *Nat Phys* 8:896–901.
23. Hunt B, et al. (2013) Massive Dirac fermions and Hofstadter butterfly in a van der Waals heterostructure. *Science* 340(6139):1427–1430.
24. Ponomarenko LA, et al. (2013) Cloning of Dirac fermions in graphene superlattices. *Nature* 497(7451):594–597.
25. Dean CR, et al. (2013) Hofstadter's butterfly and the fractal quantum Hall effect in moiré superlattices. *Nature* 497(7451):598–602.
26. Yankowitz M, et al. (2012) Emergence of superlattice Dirac points in graphene on hexagonal boron nitride. *Nat Phys* 8(5):382–386.
27. Zeng H, et al. (2013) Optical signature of symmetry variations and spin-valley coupling in atomically thin tungsten dichalcogenides. *Sci Rep* 3:1608.
28. Zhao W, et al. (2013) Evolution of electronic structure in atomically thin sheets of  $\text{WS}_2$  and  $\text{WSe}_2$ . *ACS Nano* 7(1):791–797.
29. Van Roosbroeck W, Shockley W (1954) Photon-radiative recombination of electrons and holes in germanium. *Phys Rev* 94(6):1558.
30. Kost A, Lee H, Zou Y, Dapkus P, Garmire E (1989) Band-edge absorption coefficients from photoluminescence in semiconductor multiple quantum wells. *Appl Phys Lett* 54(14):1356–1358.
31. Wilson BA (1988) Carrier dynamics and recombination mechanisms in staggered-alignment heterostructures. *IEEE J Quantum Electron* 24(8):1763–1777.
32. Li G, Zhu R, Yang Y (2012) Polymer solar cells. *Nat Photonics* 6(3):153–161.
33. Jariwala D, et al. (2013) Gate-tunable carbon nanotube- $\text{MoS}_2$  heterojunction p-n diode. *Proc Natl Acad Sci USA* 110(45):18076–18080.
34. Chuang S, et al. (2013) Near-ideal electrical properties of  $\text{InAs}/\text{WSe}_2$  van der Waals heterojunction diodes. *Appl Phys Lett* 102(24):242101.